ELSEVIER

Solid State Ionics 124 (1999) 1–19

SOLID STATE IONICS

Critical examination of the mismatch-and-relaxation frequency-response model for dispersive materials

J. Ross Macdonald*

Department of Physics and Astronomy, University of North Carolina, Chapel Hill, NC 27599-3255, USA

Received 19 November 1998; received in revised form 7 April 1999; accepted 20 April 1999

Abstract

Accurate calculations of the frequency and time responses of the new dynamic-mismatch conductive-system frequency-response model of Funke, designated by CMR, indicate that its predictions are inconsistent with some of the physically based assumptions used in deriving the model. Although it does not lead to good quantitative agreement with real-part conductivity data for $0.4Ca(NO_3)_2 \cdot 0.6KNO_3$ [CKN] for several temperatures, it may be useful for fitting other disordered or crystalline materials showing frequency dispersion. Calculation of the full complex-conductivity frequency response, not well fitted by the KWW response model, and of its unique underlying distribution of relaxation times, leads to specification of the conditions necessary for the appearance of two peaks in the frequency response of the imaginary part of the complex modulus. Important conclusions about modulus plotting and the modulus formalism fitting approach are presented, and the normalization expression used in the CMR is corrected. The appropriate expression found for the τ_0 normalization quantity, which is relevant for scaling, cannot be fully evaluated independently of experimental results. It involves a conductive-system-effective dielectric constant whose zero-frequency values, ϵ_{C0}, were found from the CKN fitting to be of the order of 10 and showed small temperature dependence. On the other hand, based on limited data, τ_0 itself showed approximate Arrhenius behavior. CMR macroscopic transient response is shown to be fitted exceptionally well by the combination of an ordinary exponential and a stretched exponential, both applying over the full time range, a type of parallel response quite different from the serial responses of the Ngai coupling model and of the closely related but more plausible distribution-of-relaxation-times cutoff model.

Keywords: Concept of mismatch and relaxation; Conductivity relaxation; Model calculations; Complex modulus

1. Introduction and background

Recently, Funke [1] and Funke and his associates [2] have presented a nearly microscopic model for dispersive frequency response of fragile glass-forming, supercooled ionic melts. This thermally-activated, conductive-system hopping model is closely related to the Funke jump relaxation model [3], does not necessarily assume the presence of fixed sites, and is based on the *c*oncept of dynamic *m*ismatch (between an ion and its neighborhood) and subsequent *r*elaxation [CMR]. When an ion hops to a neighboring position, the CMR picture assumes that a mismatch between the ion and its new neighborhood is produced, one that then relaxes. This

*Tel.: +1-919-967-5005; fax: +1-919-962-0480.
E-mail address: macd@email.unc.edu (J.R. Macdonald)

0167-2738/99/$ – see front matter
PII: S0167-2738(99)00123-X

view, as developed in Refs. [1,2], is thus very general, does not distinguish between different kinds of ions, and has been characterized by Funke as crude [1]. Nevertheless, it has led to good qualitative agreement between its predictions of the frequency and temperature dependence of the real-part of the conductivity and data on several materials, particularly calcium potassium nitrate [CKN] of composition $0.4Ca(NO_3)_2 \cdot 0.6KNO_3$. A list of definitions of acronyms and of major symbols appears at the end of this work.

To what degree may we expect the CMR, or various approximate fitting equations loosely related to it (see the discussion below), to apply beyond the area of supercooled ionic melts, such as to crystalline materials and glasses? This question is currently being addressed by Funke [4], and it is answered in part by recent work of Funke and Wilmer [5,6] where it is shown that an approximate CMR model can represent the dispersive behavior of a crystalline ionic conductor fairly closely. Although this approximate model does not lead to power-law exponent values of 0.6 or less, often found for many ionically-conducting materials, it nevertheless seems worthy of further application and analysis, particularly because it may help explain parts of the scaled master curve found for many glassy and non-glassy conductors [2,7]. The real-part conductivity master curve has a continually increasing slope of 0.7 or more which, however, never surpasses unity. Here and hereafter, 'slope' indicates the log–log slope of a quantity such as the real part of the complex conductivity with respect to frequency.

Because the CMR approach is computationally very intensive, its full quantitative response has not been investigated in detail previously. An accurate computational approach (see the Appendix) has been recently developed, however, and CMR results are discussed in some detail herein. The CMR model, complete when presented in normalized form, is based on two coupled differential equations which involve the time-dependent quantities *W*, a correlation factor which describes the motion of a central ion, and *g*, a normalized mismatch relaxation function which reflects the movements of many ions. The first equation is a part of the jump relaxation model and the second one is specific to the CMR [1,2]. Note that, as emphasized by Funke [1], the CMR approach involves moving charges only, and therefore it does not directly include dielectric-system contributions, such as that associated with the high-frequency-limiting dielectric constant, $\epsilon_{D\infty}$, arising from dipolar and vibrational effects.

The basic expression defining CMR temporal response is obtained from solution of the above coupled equations [1,2]. Let $\Theta \equiv t/\tau_x$ and $\Omega \equiv \omega\tau_x$, where τ_x is an initially undetermined characteristic relaxation time discussed in detail in Section 6.1 and there renamed τ_0. It does not appear directly in the CMR expression involving normalized variables, a reason for considering the CMR in normalized form, and the CMR approach [1,2] provides no viable expression for τ_x in terms of other parameters of the model and temperature. Thus, the CMR is not a completely microscopic model. A value of τ_x is necessary in transforming normalized CMR response to unnormalized form which can then be compared to experimental results.

Now define the important real quantity $W_N(\Theta) \equiv W(\Theta)/W_\infty$, where $W_\infty < 1$ and $W(0) = 1$, so $W_N(0)$ is just $1/W_\infty$. Thus, as Θ increases from zero, W_N decreases monotonically from $1/W_\infty$ to unity. $W(t)$ describes single-particle motion and is characterized by Funke and his associates as representing the probability that a correlated backward hop has not occurred until time t [1,2,5,6]. The translational conductivity is $\sigma(\Omega) = \sigma'(\Omega) + i\sigma''(\Omega) = \{\rho(\Omega)\}^{-1}$, where ρ is the associated resistivity. The corresponding normalized quantities are $\sigma_N(\Omega) \equiv \sigma(\Omega)/\sigma(0)$ and $\rho_N(\Omega) \equiv \rho(\Omega)/\rho(0)$. The basic CMR equation may now be written in normalized form as [1,2]

$$\Theta = E_1\{\ln[(W_N(\Theta)]\} - E_1\{\ln[(W_N(0)]\} \quad (1)$$

Here E_1 is the exponential integral of the first kind, a function which has a logarithmic singularity as its argument goes to zero. Given $W_N(\Theta)$, one can express the microscopic relaxation function, an important quantity in the derivation of Eq. (1), as [1,2]

$$g(\Theta) = \ln[(W_N(\Theta)]/\ln[(W_N(0)]. \quad (2)$$

Finally, the connection with the measurable complex conductivity may be calculated from the Fourier transform relation [3], in normalized form,

$$\sigma_N(\Omega) = W_N(0) + \int_0^\infty [dW_N(\Theta)/d\Theta] \exp(-i\Omega\Theta)d\Theta, \tag{3}$$

an equation which is consistent with the exact relations $\sigma_N(0) = 1$ and $\sigma_N(\infty) \equiv \sigma(\infty)/\sigma(0) = W_N(0) = 1/W_\infty$. It is the combination of Eqs. (1) and (3) that is here designated as the CMR model. An optimized subroutine has been added to the LEVM *c*omplex *n*onlinear *l*east *s*quares [CNLS] fitting program [8] which allows fitting of the CMR model to $\sigma(\omega)$ or $\sigma'(\omega)$ data. The parameters $\sigma_0 \equiv \sigma_{dc} \equiv \sigma'(0) \equiv \sigma(0)$, τ_x, and W_∞ may be taken free in such fitting, and, even in the absence of dielectric-system dispersion, $\epsilon_{D\infty}$ must always be included as a free or fixed parameter as well [9–13]. We shall omit primes designating the real-part of a complex quantity hereafter except when needed for clarity. Note that such quantities as $\sigma_N(\Omega)$ are nevertheless here defined as intrinsically complex, while Funke and associates do not consider $\sigma''(\omega)$ and so take $\sigma(\omega)$ as real.

Possibly because of the considerable computational difficulty inherent in using Eqs. (1) and (3) to obtain $\sigma_N(\Omega)$, Funke and his associates have usually employed their empirical *m*irror-*i*mage *a*pproach [MIA], one which follows on replacing $W_N(\Theta)$ in Eq. (1) by $\sigma'_N(\Omega)$ and Θ by $1/\Omega$ to yield

$$\Omega = [E_1\{\ln[\sigma'_N(\Omega)]\} - E_1\{\ln[\sigma'_N(\infty)]\}]^{-1} \tag{4}$$

In Ref. [2] it is stated that $W_N(\Theta)$ and $\sigma'_N(\Omega)$ ‘‘. . . are almost exact mirror images of each other when represented in log–log plots.’’ In addition, Funke also mentions that the $\sigma'_N(\Omega)$ obtained from the mirror approach ‘does not differ noticeably’ from the result obtained directly from the Fourier transform CMR approach [1]. As we shall see, however, noticeable differences between these two approaches do appear in low- and high-frequency regions, differences which render the MIA equation inconsistent with necessary physical requirements in both its limits.

In truth, the MIA is only indirectly associated, if at all, with the CMR model and should be taken to represent a different model, one which is essentially empirical and thus one which should not be associated with the physical assumptions leading to the CMR model. In fact, in their latest work [5,6], Funke and Wilmer apparently recognize this state of affairs and compare $\sigma'(\omega)$ predictions of either the MIA or an approximate version of it to data for the crystalline ionic conductor $RbAg_4I_5$. Nevertheless, in this work and even in their earlier publications [1,2], Funke and his collaborators often fail to distinguish adequately between the CMR response model, Eqs. (1) and (3) of the present discussion, and the MIA, Eq. (4), and its approximation formed by eliminating the second E_1 term in Eq. (4). They seem to include all three response equations under the rubric of the CMR physical picture. It is particularly important that these distinctions be observed so that the MIA is no longer associated with the dynamics involved in the CMR, as it is in Refs. [5,6]

One object of the present work is to investigate the adequacy of the MIA when CMR results are calculated very accurately. It is worth noting that the CMR, as defined above, yields both the real and imaginary parts of the complex conductivity $\sigma_N(\Omega)$, while the MIA is defined only for $\sigma'_N(\Omega)$, and thus no $\sigma''_N(\Omega)$ results appear in the earlier CMR work [1,2]. A more important object is to present detailed CMR frequency- and temporal-response results which shed light on the appropriateness and self-consistency of the CMR model and to develop and illustrate new aspects of its response.

2. Conductivity results and discussion

A striking feature of the CMR model is that it yields non-zero values of both $\sigma_{N\infty} \equiv \sigma_N(\infty)$ and $\rho_{N\infty} \equiv \rho_N(\infty)$. It is important to note that the high-frequency-limiting plateau defined by $\sigma_{N\infty}$ may be equal to $1/\rho_{N\infty}$, as it is for the basic CMR model, or may arise just from the presence of a limiting smallest response or relaxation time, $\tau_{\min}$. If the model response is defined by means of a *d*istribution of *r*elaxation *t*imes [DRT], always formally possible, then $\tau_{\min}$ is the low-τ cutoff end of the DRT. There will always be such a minimum response time for any real material [12,14].

Funke et al. [2] have explained the occurrence of a plateau by noting that at sufficiently high frequencies ‘‘. . . the electric field changes its sign so quickly that consecutive correlated hops would not fit into a

time window given by roughly half a cycle.'' This can be thought of as just another way of describing the presence and effects of a non-zero $\tau_{\min}$. Note that when the plateau arises solely from the presence of a non-zero $\tau_{\min}$, $\sigma_{N\infty} \neq 0$ but $\rho_{N\infty} = 0$. Even then, however, it is still the case that $\sigma_{N0} = 1/\rho_{N0}$.

All dispersive conductive-system response models lead to an effective complex dielectric constant associated only with mobile charges, $\epsilon_C(\omega)$ [9–11]. Its low-frequency limiting value, $\epsilon_{C0} \equiv \epsilon_C(0)$, may be greater or less than $\epsilon_{D\infty}$. When $\rho_{N\infty} \neq 0$, the case not only for the CMR but also for the GBEM effective-medium response model [15], it turns out that $\epsilon_{C\infty} = \epsilon_C(\infty) = 0$ [9,10], so that then $\epsilon_\infty = \epsilon(\infty) = \epsilon_{C\infty} + \epsilon_{D\infty}$ is just equal to $\epsilon_{D\infty}$ when this quantity is included in the model. But when $\rho_{N\infty} = 0$, ϵ_∞, will always exceed $\epsilon_{D\infty}$. If one deals only with the conductive-system contribution to $\sigma(\omega)$, no $\epsilon_{D\infty}$ effects are included, and thus, for the CMR, $\epsilon_\infty = 0$. It is then incorrect to include this quantity, implicitly or explicitly taken non-zero, in any equation involving only conductive-system response, as has often been done [1–3,16–20].

Suppose one introduces at the complex resistivity level a normalized frequency response function, $I(\Omega) = I'(\Omega) + iI''(\Omega)$, with $I(0) = 1$ and $I(\infty) = 0$ [9,10]. Note that $I(\Omega)$ may always be expressed in terms of a DRT; see Section 3.2. We may also write

$$\rho_N(\omega) = \rho_{N\infty} + \Delta\rho_N I(\omega) \tag{5}$$

where $\Delta\rho_N \equiv (\rho_{N0} - \rho_{N\infty})$ and $\rho_{N0} = 1$. Since $I(\infty) = 0$, the $\epsilon_C(\omega)$ response associated with $I(\omega)$ alone, namely $\epsilon_C(\omega) = 1/[i\omega\epsilon_V I(\omega)]$, will not be directly affected by the presence or absence of $\rho_{N\infty}$, and thus $\epsilon_{C\infty}$, will be non-zero. Here, ϵ_V is the permittivity of vacuum. These considerations suggest that it will be worthwhile to examine $I(\Omega)$ response as well as that of the underlying $\rho_N(\Omega)$. Note that for the CMR, or for any model for which $\rho_\infty \neq 0$, it follows from the above that

$$I(\Omega) = (\rho_N(\Omega) - W_\infty)/(1 - W_\infty), \tag{6}$$

emphasizing that $I(\Omega)$ is a quantity defined at the complex resistivity level.

Fig. 1 shows some accurate CMR and MIA $\sigma'_N(\Omega)$ plots for different W_∞ values. Also, the $I(\Omega)$ curve for $W_\infty = 0.01$ is designated by CMRI. First notice the offset between corresponding CMR and MIA curves. It turns out, as also found earlier by Funke and his associates [5,6,21], that these curves can be made to virtually coincide over most of their ranges by using a normalization in Eq. (4) different from that of the CMR but one related to it by $\tau_{\mathrm{MIA}} = (\pi/2)\tau_{\mathrm{CMR}}$, where $\tau_{\mathrm{CMR}} \equiv \tau_x$. Note in Fig. 1 that the limiting value of the CMRI curve is somewhat larger than that of the CMR but the curves are virtually the same in the low-frequency region. While the CMR plateau value is entirely determined by the value of W_∞, that for the CMRI involves a quotient of two moments of the DRT associated with the $I(\Omega)$ response [9,10].

Although shifted MIA response is very close to

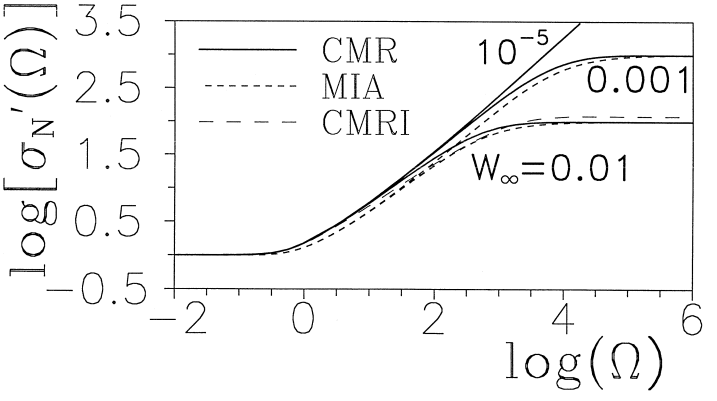

Fig. 1. Log–log plots of the real part of the normalized conductivity $\sigma'_N(\Omega) \equiv \sigma'(\Omega)/\sigma_0$ vs. normalized frequency, $\Omega \equiv \omega\tau_x$. Shown is the response for the dynamic mismatch relaxation model (CMR), the mirror approach (MIA), and the (CMRI) $I'(\Omega)$ response calculated from the $\sigma'_N(\Omega)$ CMR response, using Eq. (6), and then transformed to the complex conductivity level. Here, $W_\infty = \sigma_0/\sigma_\infty \equiv 1/\sigma_{\infty N}$.

the real-part response of the CMR in its middle, high-slope region, differences which are not very apparent on a log–log scale are clearly visible when one plots the slopes themselves. Fig. 2 shows such results for $W_\infty = 0.001$, ones where the MIA response has not been shifted. The CMR and MIA curves at the bottom of the graph appear very close to one another except for the MIA frequency shift. But the actual slopes of the response at low and high frequencies are obscured by the non-zero limiting values in these regions. When we subtract one from the original data before calculating the slopes, we obtain the curves marked CMRSL and MIASL, while if we subtract σ_N' from $\sigma_{N\infty} = 1/W_\infty$ and then calculate the slopes, we obtain negative values. For ease of comparison, the absolute values of these high-end slopes are plotted in Fig. 2 and identified by CMRSH and MIASH. These results for the intrinsic underlying response show that the CMR properly involves a limiting low-frequency slope of 2, while the MIA's slope approaches infinity in this limit. Similarly, at high frequencies, the intrinsic CMR slope is -2 but that of the MIA only approaches -1. Thus in both cases the MIA leads to physically unrealizable results.

Funke et al. [1,2] have noted that the (unsubtracted) slope of a version of the MIA in which the right E_1 term in Eq. (6) is omitted (a new approximate MIA model) increases continuously as the frequency is increased but never reaches unity. Somewhat different behavior applies for the CMR (and the complete MIA). As shown in Fig. 2, the slope reaches a maximum as the frequency increases and then decreases toward zero. The smaller the value of W_∞, the higher the maximum slope. For example, the maximum values for 0.01, 0.001, 10^{-5}, and 10^{-8} are found to be approximately 0.69, 0.79, 0.88, and 0.93, respectively.

Fig. 3 shows the frequency dependence of the $\sigma_N''(\Omega)$ response associated with that of the $\sigma_N'(\Omega)$ presented in Fig. 1. It is important because it verifies assertions made above that the CMR, being a purely conductive-system model, includes no non-zero $\epsilon_{D\infty}$, and also that $\epsilon_{C\infty} = 0$ because $\rho_{N\infty} \neq 0$. The two CMR curves reach maxima and then decrease with a limiting slope of -1. Such behavior is associated with $\epsilon_C(\omega)$, and the continued decay occurs because $\epsilon_{C\infty} = 0$. Further, Monte Carlo simulations for structurally disordered ionic models, ones without $\epsilon_{D\infty}$ included, exhibit curves of the same shape [22,23].

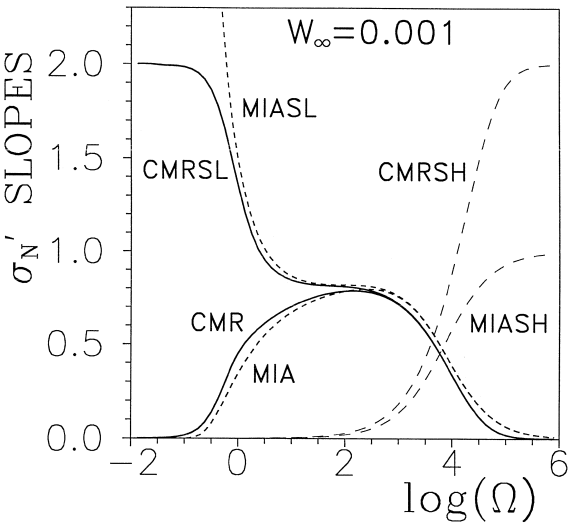

Fig. 2. Slopes of $\sigma_N'(\Omega)$ without and with subtraction of plateau values before slope calculation. Here 'SL' identifies subtraction of the low-Ω plateau value, and 'SH' denotes subtraction *from* the high-Ω plateau value. The high-end curves designated as CMRSH and MIASH show the negatives of the actual high-end slopes.

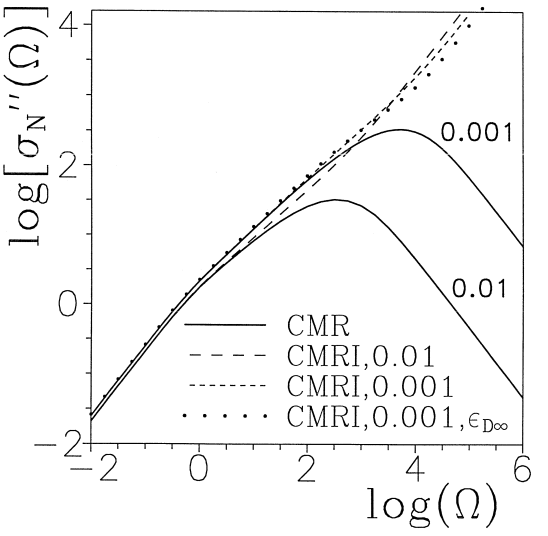

Fig. 3. Log–log plots of the imaginary part of the normalized conductivity vs. normalized frequency. In addition to the two CMR curves shown, two corresponding CMRI $I''(\Omega)$ conductivity curves are presented, as well as a third which includes the effects of an $\epsilon_{D\infty}$ contribution with $\epsilon_{D\infty N} \equiv (e_V/\sigma_0\tau_x)\epsilon_{D\infty} = 0.1$.

In contrast, the CMRI curves in the figure, for which $\epsilon_{C\infty} \neq 0$, show some slope changes but no maxima. For the dotted CMRI curve, a value of $\epsilon_{D\infty N} = 0.1$ was included in calculating the original data. This small value evidently does not produce a large change in the $I(\Omega)$ response, but would entirely change the character of the CMR response. Here we define $\epsilon_N \equiv 1/M_N = \sigma_N/i\Omega$, where the normalized complex modulus is $M_N(\Omega) = M'_N(\Omega) + iM''_N(\Omega)$. It follows that $\epsilon_{D\infty} = (\sigma_0\tau_x/\epsilon_V)\epsilon_{D\infty N}$.

Since the MIA involves only real-part normalized conductivity response, one cannot directly calculate the complex $\rho_N(\Omega)$, $M_N(\Omega)$, and $\epsilon_N(\Omega)$ responses associated with it. Even though the MIA does not define the $\sigma''_N(\Omega)$ response associated with its $\sigma'_N(\Omega)$ response, there is a way to obtain it, as described in Section 4. Fig. 4 shows, however, only complex-resistivity-plane results for the CMR. For $W_\infty \leq 0.01$, there would be little visible difference between $\rho_N(\Omega)$ and $I(\Omega)$ response curves, but the difference becomes extreme as $W_\infty \to 1$. For example, for $W_\infty = 0.9$ the $\rho_N(\Omega)$ curve would appear only between $\rho'_N = 0.9$ and 1, while the corresponding $I(\Omega)$ curve, designated here as $0.9I$, approaches very close to the semicircular shape of simple Debye response.

It is of interest to evaluate how well CMR response can be fitted using the *K*ohlrausch–*W*illiams–*W*atts (KWW) response model [24–26], one which has been derived from various physical assumptions and found to represent a large body of data quite well [9–11,27,28]. In the time domain, it involves fractional exponential behavior of the form

$$\phi(t) = \exp[-(t/\tau_K)^\beta],\ 0 < \beta \leq 1. \tag{7}$$

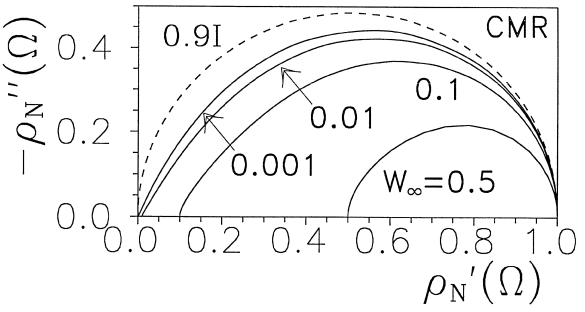

Fig. 4. Complex-resistivity-plane results for ρ_N and four values of W_∞. The curve marked $0.9I$ shows the $I(\Omega)$ response for $W_\infty = 0.9$. Here frequency increases parametrically from right to left.

Although no closed-form expression exists for KWW frequency response with arbitrary β, such a response can be calculated numerically with very high accuracy and is available in the LEVM program [8], including both the conventional KWW model and a cut-off modification of it, one which restores physical realizability to the response [12–14].

KWW fitting of full complex CMR frequency–response data for $W_\infty = 0.001$ and $0.001 \leq \Omega \leq 10^6$, yielded a rather poor fit, with the standard deviation of the relative residuals, S_F, equal to about 0.084. Let $\tau_{KN} \equiv \tau_K/\tau_x$ be a free parameter of the fit of the normalized CMR data. Fitting led to an estimate of τ_{KN} of about 2.3, compared to the value of unity inherent in the normalized CMR model itself. Its estimates of $\Delta\rho_N$ and $\rho_{N\infty}$ were excellent, however, and the estimates of β and $\tau_{N\min} \equiv \tau_{\min}/\tau_x$ were about 0.75 and 5.5×10^{-6} respectively. No adequate fit was obtained when the free parameter $\rho_{N\infty}$ was fixed at zero. On the other hand, fitting without DRT cutoff led to an appreciably worse fit than the above one and to a poorer estimate of $\rho_{N\infty}$. These results indicate that the KWW model, even with an added $\rho_{N\infty}$ free parameter, differs appreciably from the CMR model. In contrast, it has been shown [29] that the Funke jump relaxation model, to which the CMR model is closely related, does lead to KWW behavior.

Fitting of only the $\sigma'_N(\Omega)$ data to the KWW model led to smaller values of S_F, another indication of differences between the models. Here, with both $\rho_{N\infty}$ and the cutoff parameter simultaneously free to vary, fitting led to the no-cutoff condition; S_F was about 0.056; and the β estimate was about 0.74. Surprisingly, when $\rho_{N\infty}$ was fixed at zero, the smaller value $S_F \simeq 0.035$ was obtained with $\tau_{N\min} \simeq 2.38\times10^{-5}$ and $\beta \simeq 0.81$. Since the CMR data involve both a non-zero $\rho_{N\infty}$ and low-τ cutoff, however, it is clear that complex fitting yields a better picture of the situation here than does real-part fitting. Finally, fitting of the CMR data with the MIA model yielded a value of $S_F \simeq 0.015$ and an estimate of $\tau_{\mathrm{MIAN}} \simeq 1.52$, rather than the value of $\pi/2$ mentioned above. When the fitting was restricted to the middle region, $10 \leq \Omega \leq 100$ however, a value of about 1.555 was obtained. Although the MIA is clearly useful for preliminary fitting of putative CMR data, the CMR model itself should be used for final fitting, par-

ticularly if random errors in the data are of the order of one per cent or less.

3. Modulus plots and modulus formalism

3.1. Important modulus-related distinctions

Over the years there has been a great deal of discussion about the appropriateness of using the electric modulus or not [e.g., [18–20,30–33]]. A crucial distinction, which is often not recognized or defined [30–33], is that between modulus plots [plotting data in terms of $M'(\omega)$ and $M''(\omega)$] and the modulus formalism, an approach which is not a matter of plotting but is a method of generating a new response model from a known one [9–11,16,17]. Often (but not here) the term 'modulus formalism' is used to mean either or both of the above. Failure to recognize this distinction renders some of the previous discussions of these matters somewhat moot.

It is important to note that data can be plotted at any of the four immittance levels. None of them should be given a favored place at the expense of the others, and data analysis should properly begin with plots of the data at all four levels. The electric modulus was perhaps first introduced by Shrama [34], and it has been stated by Angell [30] to have been invented to eliminate electrode polarization, although this was not Shrama's aim. For some this is an advantage [18–20,30], for others a disadvantage [30,33]. This interpretation is, however, based on a misconception. As compared to plotting at the complex resistivity level, modulus plotting of the same data tends to hide low-frequency effects, but it does not eliminate them. In fact, CNLS fitting of the data transformed to either of these two levels yields exactly the same parameter estimates when proportional weighting is employed [8]. Therefore, criticisms based on the character of modulus plots or on their analysis [30,33], ones which even challenge the physical basis of the modulus, are inapplicable when adequate analysis methods are applied.

Dyre [31] has implied that data expressed at the modulus level cannot be related to a significant DRT, one related to the motion of mobile charges. This was an important insight at the time he wrote, a time when the ubiquitous presence of $\epsilon_{D\infty}$, was not generally included properly in data analyses. But note that since a data set still contains the same information independent of which of the four immittance levels it is expressed at, Dyre's remark, if it were applicable, would apply for any of these levels. Experimental immittance data sets always include effects arising from $\epsilon_{D\infty}$, so any DRT derived from the data without explicit consideration of $\epsilon_{D\infty}$ will include such effects and will not represent the true conductive-system DRT [9,10,31]. Similarly, the use of any fit model which does not account properly for $\epsilon_{D\infty}$ is guaranteed to lead to incorrect results [11]. This effect was, unfortunately, not recognized by Moynihan and associates [16–20], resulting in poor estimates of some fitting parameters and misinterpretation of data by those who have used the original modulus formalism [16,17] for data analysis. Recent work has quantified this problem and shown how it may be entirely avoided through the use of CNLS fitting with $\epsilon_{D\infty}$ taken as a separate free parameter in either direct fitting or in data inversion to estimate a DRT [9–13].

3.2. Modulus-formalism models and modulus response

In order to describe the original [16,17] and corrected modulus–formalism response models [9–11], first let $x \equiv \tau/\tau_x$ and define $y \equiv \ln(x)$. Further, define a normalized DRT for a particular response model as $G_n(x)$, where $n = 0$ or 1. We may now write, for two kinds of response defined by the value of n,

$$I_n(\Omega) \equiv \int_0^\infty \frac{G_n(x)\mathrm{d}x}{[1 + i\Omega x]} = \int_{-\infty}^\infty \frac{F_n(y)\mathrm{d}y}{[1 + i\Omega \exp(y)]}, \qquad (8)$$

and $F_n(y) = xG_n(x)$ from conservation of probability. For the moment we follow convention and assume that the above distributions do not include any effects arising from a non-zero ρ_∞; therefore when it is non-zero, Eq. (5) is applicable. If the choice $n = 0$ specifies a known response model $I_0(\Omega)$, for example the KWW, here now designated as KWW0, then it turns out [9–11] that the corresponding modulus-formalism model, $I_1(\Omega)$, is just defined by Eq. (8) with $n = 1$ and

$$G_1(x) = [x/\langle x\rangle_0]G_0(x). \tag{9}$$

Finally, the dimensionless moments of a distribution are given by:

$$\langle x^m\rangle_n \equiv \int_0^\infty x^m G_n(x)\mathrm{d}x, \tag{10}$$

with m an integer and the average relaxation time for the distribution is $\langle\tau\rangle_n = \tau_{xn}\langle x\rangle_n$. Note that the dimensionless quantities in Eq. (10) do not depend directly on τ_x but only on the shape of the distribution.

The above relations are sufficient to allow one to write the connection between I_1 and I_0 as [9–11]

$$I_1(\Omega) = [1 - I_0(\Omega)]/[i\Omega\langle x\rangle_0]. \tag{11}$$

In previous work, the $\langle x\rangle_0$ in Eq. (11) has often been replaced by $1/\langle x^{-1}\rangle_1$, but this relationship only applies when the same parameter values are used for separate $n=0$ and 1 response calculations [13], and it is inapplicable when one fits the same data set with the $n=1$ model following from a given $n=0$ one, as in Eq. (11) [11]. Its failure ensures that the relation $(\epsilon_{C0})_0 = (\epsilon_{C\infty})_1$, also used previously, then fails as well.

Note that $I_1(\Omega)$, like $I_0(\Omega)$, is defined at the complex resistivity level but can be transformed to any of the three other levels. From this point of view, $I_1(\Omega)$ is not particularly a modulus-related quantity. Therefore, instead of defining $I_0(\Omega)$ and $I_1(\Omega)$ as describing ordinary and modulus formalism responses, it is more appropriate to identify them as different kinds of *c*onductive-system *d*ispersion (CSD) response. CSD0 and CSD1 [11–13]. Because CSD0 and CSD1 models are different and yield different frequency response, their associated time responses are also different. Thus, the fractional-exponent temporal response of the KWW0 model, Eq. (7), is quite different from that for the KWW1 model, even though the models are related as above [12]. In Section 6.1, it will be shown how the original modulus-formalism response is related to Eq. (11). Incidentally, the KWW fitting results discussed in the last section used the ordinary CSD0 KWW0 fitting model, and only much worse fits could be obtained with the CSD1 KWW1 response model.

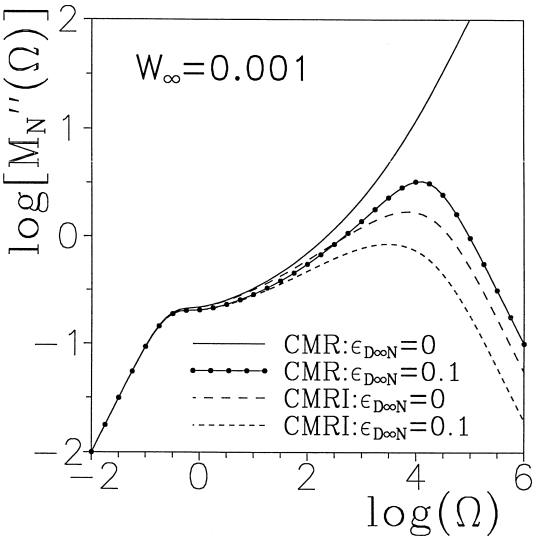

Fig. 5. Log–log plot of the imaginary part of the normalized complex modulus, $M_N''(\Omega)$, with and without some effects of $\epsilon_{D\infty}$ included. Here, $M_N(\Omega) \equiv i\Omega\rho_N$.

Fig. 5 presents some normalized modulus-level CMR and CMRI response curves. The top CMR curve shows that $M_N''(\Omega)$ increases indefinitely with increasing frequency, an indication that $\epsilon_\infty = 0$. For the three lower curves, however, $\epsilon_\infty \neq 0$ and a peak appears. A curve like the basic CMR one here has been presented for CKN data at 453 K [35]. Although it shows $M''(\omega)$ increasing at its high-frequency end, as does the present CMR curve, the results are characterized in Ref. [35] as involving two maxima. And, in fact, since $\epsilon_{D\infty} \neq 0$ for real data, a peak must indeed appear beyond the highest frequency shown. Interestingly, some disordered-system Monte Carlo results do show one or two peaks even though the presence of any $\epsilon_{D\infty} \neq 0$ is not stated [36]. Further, independent CKN measurements [37] did not confirm two-peak behavior, possibly because of the absence of sufficient high-frequency data. Factors instrumental in producing two peaks will be discussed in Section 4.

4. Distribution estimates

The LEVM program allows one to estimate the DRT associated with a set of frequency- or time-response data [8–10,12,13,38–40]. It can provide estimates of any discrete distribution points and of continuous ones, yields unambiguous discrimination between them, and, when the DRT contains both discrete points and a continuous part, leads to a set of $\{e_i, y_i\}$ points of a normalized distribution, $F_{DC}(y_i)$, with $1 \le i \le N$. Here, the strength parameters e_i are denoted d_i for discrete points not a part of any continuous DRT and are denoted by c_i for discrete points which define the continuum part of the DRT. Unlike other inversion approaches, that in LEVM permits both the e_i and y_i (or x_i) quantities to be free parameters of the fit. This, in turn, allows unambiguous discrimination between the two types of response. Although the continuum parts are necessarily represented by discrete points, discrimination between c_i and d_i responses is achieved by observing results for different N values: the y_i values for continuum points vary with N while those for any non-continuum discrete points do not.

In order to take simultaneous account of all d_i discrete points of a distribution, especially that associated with the presence of ρ_∞, and continuous contributions, we may write $\rho_N(\Omega) = I_{DC}(\Omega)$ instead of Eqs. (5) and (6). Then, Eq. (8) necessarily involves the full DRT, $G_{DC}(x)$ or $F_{DC}(y)$, normalized so that $I_{DC}(0) = 1$. Fig. 6 shows $n = 0$ results for some of the present CMR and CMRI data. Because a logarithmic τ scale is used, the results are those associated with $F_{DC}(y)$ rather than with $G_{DC}(x)$. In much previous work [e.g. [16,17], this distinction has not been recognized [9,10,12,13].

The fits that led to the present inversion estimates were exceptionally good. For example, the CMR curve with $N = 19$ yielded $S_F = 8 \times 10^{-7}$. For each of the two CMR curves, a discrete-DRT point has not been shown because it involves too small an x value. Values for the two points are $\{d_1, x_1\} = 4.9 \times 10^{-4}$, 2.2×10^{-14} and 1.6×10^{-4}, 5.0×10^{-31} for $W_\infty = 0.001$ and 0.01, respectively. When these points are either directly eliminated from the fit or when CMRI frequency response calculated by Eq. (6) is inverted, one finds that all ρ_∞ effects are eliminated. Thus, the presence of a non-zero ρ_∞ in the CMR model contributes a term $\delta(y - y_1)$ to the full distribution. Here, δ denotes the Dirac delta function, and one would expect that $x_1 = \exp(y_1)$ should be zero. Although the x_1 values cited above are not zero, they are very small, and, in addition, their estimated relative standard deviations are very large, allowing these x_1 estimates to be taken consistent with zero.

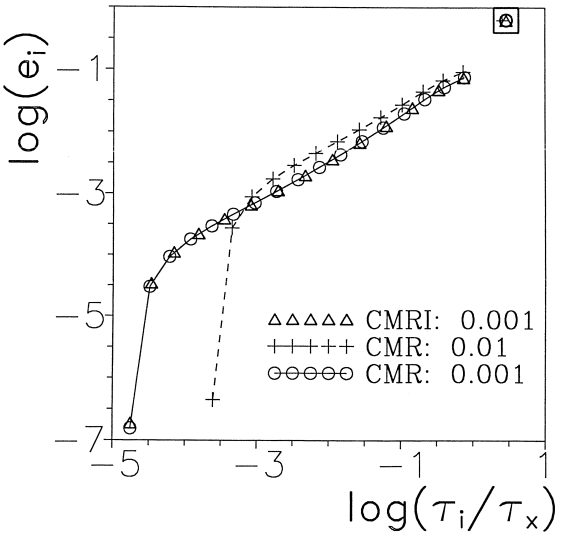

Fig. 6. Log–log behavior of CMR and CMRI distributions of relaxation times. Here, the e_i quantities are values of the strength parameters of the distribution. Low-τ and high-τ cut-offs of each continuous distribution are apparent, as well as an isolated point at the high-τ end of the distribution. Another isolated discrete point is a part of the CMR but not the CMRI distribution, but it falls at much too low values of τ_i/τ_x to plot here (see text).

Fig. 6 shows that the CMR and CMRI F_{DC}'s involve a continuum part, the usual situation, as well as a second d_i discrete point (shown inside the large square-box symbol). For the CMR model, the c_i continuum points are those defined by $2 \le i \le (N - 1)$, and the high-end discrete point is specified by $i = N$ for both the CMR and the CMRI. Note that although the c_i points fall approximately on a straight line over much of their range, the slope of the continuum response is not constant but is continuously varying. Further, the results show that this part of the response is cut off both at its low-x and at

its high end. No increase in N causes the c_i points to lie outside the range shown. The values of x_2 for the CMR and x_1. for the CMRI, which are both $x_{\min}$ for this part of the distribution, are about 1.75×10^{-5} and 1.76×10^{-5}, respectively, for $W_\infty = 0.001$. As one would expect, the continuum distribution is narrower for $W_\infty = 0.01$ as it begins to approach simple Debye behavior. It is worth remarking that the $\langle x\rangle_0$ estimates obtained from the inversion for $W_\infty = 0.001$ are $2.50999 = 0.999\times2.51250$ and 2.51250, for the CMR and CMRI, respectively. For $W_\infty = 0.01$, the CMR estimate was 2.1062.

For $W_\infty = 0.001$, the $\{d_N, x_N\}$ points for the CMRI and CMR are 0.61809, 2.9062 and 0.62858, 2.9065, respectively. The x_N values are the same, in spite of the different N values used, and the d_N ones differ because the effective W_∞ is actually somewhat less than 0.001 for the CMRI, as shown in Fig. 1. This discrete point contributes a term $\delta(y - y_N)$ to the full distribution. It leads to the dominant part of $\rho_N(\Omega)$ response at low frequencies. The presence of two d_i discrete points as well as a continuum part makes CMR distributions unique in the present author's experience.

Once a DRT which represents the data to high accuracy has been obtained, it is straightforward to use it in LEVM to generate model data with any DRT point or points eliminated. This facility can be employed to investigate the factors leading to the unusual two-peak $M''(\Omega)$ response discussed in the last section. We find that with the full DRT, plus a value of $\epsilon_{D\infty N}$ of about 0.95, two peaks of nearly equal height appear, with an appreciable valley between them. This value of $\epsilon_{D\infty N}$ is experimentally reasonable because, for the CKN data analyzed in Section 6.2, we may use the fit parameters found for temperatures of 478 K and 423 K to convert the plausible value of $\epsilon_{D\infty} = 5$ to the corresponding $\epsilon_{D\infty N}$ values, yielding results close to 0.95. On the other hand, generation of $M''(\Omega)$ curves with one or both of the isolated discrete end points of the full distribution eliminated yields only distorted single-peak response for any values of $\epsilon_{D\infty N}$. It thus appears that two-peak response is a characteristic feature of the full CMR response when and only when a plausible non-zero value of $\epsilon_{D\infty}$ is included. Finally, it is worth noting that two peaks have been found for a polycrystalline lithium aluminosilicate material and ascribed to bulk effects [41], and some evidence of two peaks appears in results for intercalated polymer electrolytes [42]. It is thus likely that different processes may lead to two-peak behavior, a matter worthy of further investigation.

5. CMR temporal responses

When one has available an expression for a DRT, one can readily calculate the macroscopic temporal response $\phi(t)$ (termed $G(t)$ by Funke and associates [1,2]) associated with it [9,10,12,13,38,39]. The present CMR DRT is defined, as discussed in Section 4, by up to 19 e_i values, each of which leads to simple Debye response in the frequency domain and to a corresponding number of weighted exponentials in the time domain. Since the estimated CMR DRT was able to represent the frequency-response data so accurately, it is highly likely that any temporal response calculated from it will be correspondingly accurate and appropriate, in spite of the generally ill-posed character of inversion results for a continuous distribution.

Fig. 7 shows a comparison between the $W_\infty = 0.001$ $g(\Theta)$ response defined by Eq. (2) and the

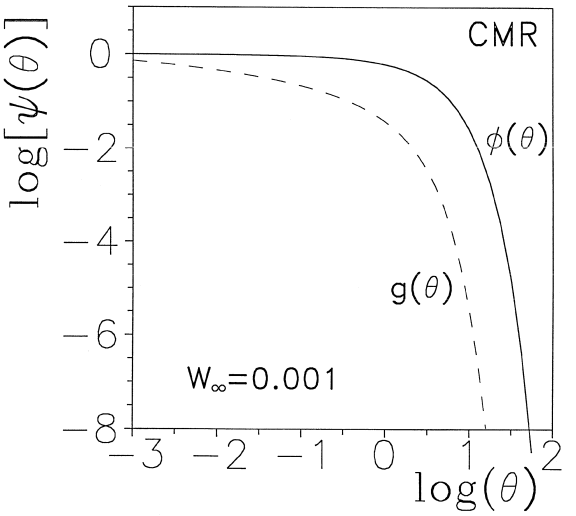

Fig. 7. Comparison of the temporal response of the microscopic response function $g(\Theta)$ with the corresponding macroscopic function $\phi(\Theta)$, where the normalized time is $\Theta \equiv t/\tau_x$. The function ψ is either g or ϕ.

corresponding $\phi(\Theta)$ response calculated from the DRT. It is worth noting that Eq. (2) follows from the original Funke jump relaxation model [3], but only when $W_\infty < 1$. When $W_\infty = 1$, one obtains just $g(\Theta) = \exp(-\Theta)$, consistent with the resulting simple Debye response of $\rho_N(\Omega)$.

Clearly, there are large differences between these microscopic and macroscopic responses. In Refs. [1,2], Funke and his associates have pointed out that $g(t)$ and $W(t)$ do not properly describe mismatch relaxation at short times, and they discussed possible reasons for such failure from a microscopic point of view. But the present results show large differences over the full range, not just at the short-time end of it. This is particularly important because the derivation of the CMR, Eq. (1), is founded on the assumption $g(\Theta) = \phi(\Theta)$ [1,2], a physically based relation between the many-particle relaxation function $g(\Theta)$ and the macroscopic relaxation function $\phi(\Theta)$ [2]. Although this approximation, which ignores ''the properties of the relaxing neighborhood which cannot be described in terms of moving charges,'' is characterized as crude [1], it nevertheless is a crucial part of the derivation of Eq. (1).

The failure of the above equation to apply, not only at short times but over the full temporal range, indicates that the theoretical basis of the CMR model of Eq. (1) is questionable and its connection with the microscopic differential equations used to derive Eq. (1) is flawed. Therefore, it appears that not only the MIA response model but also the present CMR model should be taken more as an empirical fitting equation rather than as a firm deduction from plausible microscopic physical processes.

It is worth noting that in [5,6], whose analysis is based on the MIA, the authors emphasize that the time derivative of the present Eq. (2) is ''the central relation of the CMR,'' a result that ''states that the rates of relaxation via single and many particle routes are coupled to each other in a synchronous fashion.'' Although this is an important part of the Funke jump relaxation model [3], the results above and the disconnection between the MIA and the CMR, as defined by Eqs. (1) and (3), indicate that both the CMR and the MIA should be treated as empirical fitting models, inconsistent with Eq. (2). Although Funke and Wilmer [5,6] emphasize that this central relation was derived in their work by analysis of experimental spectra, they consider no time-dependence data directly and only compare frequency-response data with MIA, or approximate MIA, predictions. Thus, the connection they claim to the CMR and to its Eq. (1) response model seems tenuous.

Finally, Funke and Wilmer suggest that the approximate MIA model, which predicts a slope continuously increasing toward, but not reaching, unity, is appropriate for describing the nearly constant loss (NCL) behavior which appears for some ion conducting materials at low temperatures (e.g., see [43,44]). But such behavior generally appears at sufficiently low temperatures that the charge carriers may not be completely dissociated. When this is the case, it is improper to use the Nernst–Einstein relation to transform from normalized conductivity to a normalized angular-frequency-dependent coefficient of self-diffusion, as in Eqs. (5) and (8) of Ref. [5,6]. Further, even if the approximate MIA model led to an adequate fit of such data, little or no light would be shed thereby on the physics of the processes involved since the MIA is empirical.

It is of interest to see how well the two responses of Fig. 7 can be separately fitted in the time domain. A remarkably good fit of the $\phi(\Theta)$ data, extending over the Θ range from 0.001 to 100, was obtained on using the function

$$\phi_F(\Theta) = A\exp(-\Theta/B) + C\exp[-(\Theta/D)^E]. \qquad (12)$$

The S_F value for the fit was 6.8×10^{-4}, and the relative standard deviations of the five parameters were all smaller than 0.004. In alphabetical order, the estimates obtained were about 0.8363, 2.9067, 0.1611, 0.40608, and 0.7281, respectively. Note that the value of B is virtually exactly the same as that of x_N listed above for the largest discrete point of the CMR DRT. It is therefore clear that that isolated-point contribution to the DRT is associated with a large exponential contribution to the temporal response. Furthermore, D^{-1} is close to the CMR $\langle x\rangle_0$ value also listed in the last section. The fitting function of Eq. (12) led to a very poor fit of the $g(\Theta)$ data, especially at the low-Θ end. When the data are restricted to the range shown in the figure, one obtains a value of S_F of about 0.1 and the following parameter estimates: 0.414, 0.046, 0.172, 0.696, and

0.895. When the range began at $\Theta = 1$, an appreciably smaller value of S_F was found with, most significantly, both D and E estimates very close to unity: ordinary exponential response. Incidentally, for fitting of the $\phi(\Theta)$ data with the Θ range again beginning at unity, estimates of D and E were 0.59 and 0.90, changing to 0.77 and 1, respectively, when the data began at $\Theta = 10$.

Since the DRT approach makes it easy to eliminate any of the individual points of the DRT fit of the data, one can readily generate $\phi(\Theta)$ synthetic data with the two isolated d_1-type discrete points of the full distribution eliminated, leaving only the continuous part of it; denote the result by $\phi_T(\Theta)$. It makes no significant difference whether or not the small-τ point is eliminated, but elimination of the large-τ one leads to quite different results when Eq. (12) is used for fitting the $\phi_T(\Theta)$ data. The resulting S_F value was about 0.015, indicating a pretty good fit but one far inferior to the principal one discussed above. The parameter estimates were about 0.0486, 0.7762, 0.0854, 0.1986, and 0.7877. The continued need for a simple exponential contribution to the response, as demonstrated here, arises from the cutoff of the continuous distribution at its low-τ end [12].

These results show that even the continuous part of the DRT does not lead to excellent KWW0 fractional exponential response. More can be learned by plotting in a way that would lead to a straight line with a slope of β if Eq. (7) applied. Following Funke [3], one obtains the results of Fig. 8, where ψ is either ϕ, ϕ_T, or g, and an ordinary log function in Fig. 33 of Ref. [3] has been replaced by a natural log. Further, it is also essential for the $\phi_T(\Theta)$ plots that $\phi_T(\Theta)$ be renormalized so that $\phi_T(0) = 1$. In Fig. 8 all the limiting slopes of the curves, except that of $\phi(\Theta)$ at its low end, have values of unity, indicating ordinary exponential response. Unlike the corresponding jump-model curve in Ref. [3], which shows such limiting behavior at both ends, the CMR only does so at the high end. It appears from this figure that none of the curves show much of a region of constant slope less than unity, but the matter may be made clearer by plotting the quantity $\eta \equiv d\{[\log[-\ln\{\psi(\Theta)\}]\}/d\{\log(\Theta)\}$ vs. $\log(\Theta)$ as in Fig. 9. In this representation [12], Eq. (7) would lead to a horizontal line with η equal to the value of β. We see

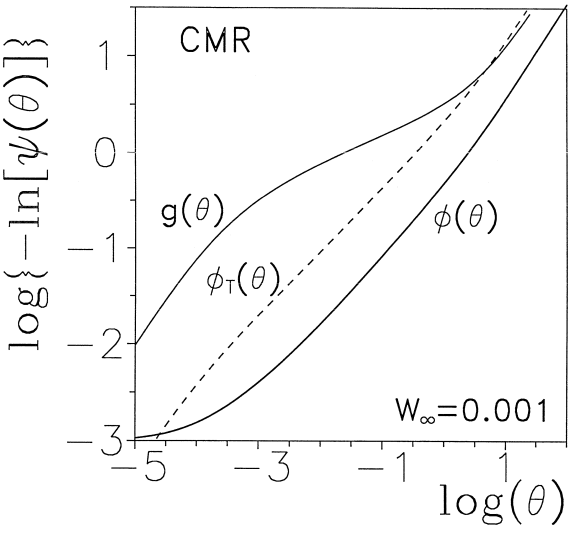

Fig. 8. Plots of time–response functions using an ordinate transformation which would result in a line of constant slope β if the normalized stretched-exponential function of Eq. (7) applied. Here ϕ_T is the normalized response following from only the continuous part of the CMR distribution of relaxation times.

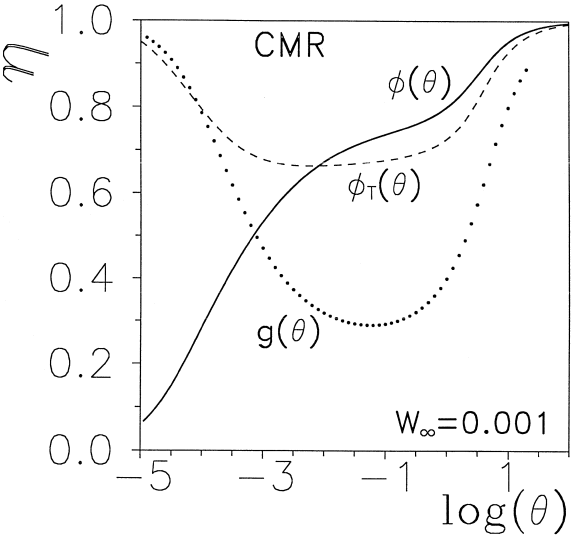

Fig. 9. Plots of $\eta \equiv d\{[\log[-\ln\{\psi(\Theta)\}]\}/d\{\log(\Theta)\}$ vs. $\log(\Theta)$. Here normalized stretched-exponential response leads to a horizontal line at $\eta = \beta$.

that there is only a relatively small region with a nearly constant value of about 0.67 for the $\phi_T(\Theta)$ curve.

It is worth emphasizing the difference between the

present CMR temporal response and that of the Ngai coupling model or the cutoff model. In the coupling model [see Ref. [12] for many references and discussion], KWW0 temporal response is employed for times, t_c, longer than about 10^{-12} s and simple exponential response is grafted on for times equal-to and shorter than this. The more reasonable cutoff approach [9,10,12] shows a smooth transition in the time domain from any appropriate response model in the region near t_c to exponential response, automatically produced by a cutoff of the continuous DRT of the model at $\tau_{\min} = t_c$. No d_1 discrete points are necessarily part of the complete DRT. On the other hand, CMR response involves two discrete points lying outside a continuum DRT region. Further, as we have seen from the above fitting results, $\phi(\Theta)$ can be very well represented by the sum of a simple exponential and a fractional exponential. Therefore, its response is necessarily different from that of, for example, a KWW0 fractional-exponential model with cutoff [12], which, in some sense may be considered serial response, as opposed to the parallel response of the CMR model.

6. Data fitting and limitations of the CMR model

6.1. Normalization of time and frequency

Richard Feynman said, ''Experiment is the sole judge of scientific truth.'' Thus, in attempting to understand and explain some aspect of nature by means of a response model, model predictions must be compared with experimental results in order to evaluate the strengths, weaknesses, and domain of applicability of the model, itself always an idealization.

Funke has made the remarkable claim that the full unnormalized frequency response of the CMR, $\sigma'(\omega)$, approximated by the mirror approach, may be calculated when the dc conductivity is known, and he has provided simulation examples using CKN data for five different temperatures, T [1]. Actually, he found that CKN $\sigma_\infty(T)$ values were thermally activated, and he used experimental estimates of $\sigma_\infty(T)$, $\sigma_0(T)$, and the mirror approach (Eq. (4) herein) to calculate $\sigma'_N(\Omega_\sigma, T)$ as a function of the normalized frequency, defined by $\Omega_\sigma \equiv \omega\langle\tau_\sigma(T)\rangle$. A specific value of the quantity $\langle\tau_\sigma(T)\rangle$, which was additionally needed to unnormalize the results, was obtained by using the 'conductivity relaxation time' expression [16–20,45]:

$$\langle\tau_\sigma\rangle = \epsilon_V\epsilon_\infty/\sigma_0, \tag{13}$$

with a value of 7 taken for ϵ_∞. Note that it is often not stated when this equation is used whether $\epsilon_\infty = \epsilon_{C\infty} + \epsilon_{D\infty}$ or whether it is equal to just $\epsilon_{D\infty}$, although the latter choice was employed in the original modulus–formalism treatment [16,17], one where the existence of $\epsilon_C(\omega)$ was unrecognized.

There are several problems with the above procedure. First, the results pertain to the MIA model, rather than to the exact CMR model, although Eq. (13) was used for both in Refs. [1,2]. In current work of Funke and his associates [5,6], however, the τ_x, or its equivalent, appropriate for the MIA has been adjusted so that it is $\pi/2$ times larger than that for the CMR, making the σ' curves for the two approaches very nearly agree over most of their frequency span, as discussed earlier herein in regard to Fig. 1. Further, although in Ref. [5,6] Funke and Wilmer have actually entirely eschewed the use of Eq. (13) by writing $\Omega_\sigma = \omega/\omega_{\text{onset}}$, where $1/\omega_{\text{onset}}$ is proportional to the present τ_x, a quantity which must be determined experimentally until a valid theory for it is available, we shall continue to discuss Eq. (13) and its corrections below because it has been so widely used in the past.

Secondly, as shown in Section 2, $\epsilon_\infty = 0$ for a conductive-system model with $\rho_\infty \neq 0$, such as the CMR, where no $\epsilon_{D\infty}$ value has been included. Therefore, Eq. (13) is inapplicable, and it must be replaced by the proper conductive-system result appropriate for $\rho_\infty \neq 0$ [9–11], one where we set $\tau_x = \tau_0$ so that the appropriate normalized frequency is $\Omega = \omega\tau_0$ and the corresponding normalized time response will involve $\Theta \equiv t/\tau_0$. The following equations for τ_0 are general and apply to all $n = 0$ conductive-system dispersive response models which either do or don't include a series ρ_∞.

Let us consider CSD0 behavior but omit the 0 subscript for simplicity when it is not explicitly needed and use an 'S' subscript to denote situations with $\rho_\infty \neq 0$. Then $\langle x\rangle \equiv \langle x\rangle_0$ is the average, or first

moment, for a CSD0 model without ρ_∞, an average using just the DRT of the dispersive part of the response, herein denoted as $I(\Omega)$ for a conductive system, and $\langle x\rangle_S$ identifies the corresponding average for a model with $\rho_\infty \neq 0$, such as the present CMR. It is worth noting that for normalized response, $\langle x\rangle$ need not be calculated from the pertinent DRT but is given by the limit of $\Omega^{-1}\sigma_N''(\Omega)$ or of $\Omega^{-1}\rho_N''(\Omega)$ as $\Omega \to 0$ when ρ_∞ and $\epsilon_{D\infty}$ effects are not included in the data set.

For the $\rho_\infty = 0$ situation, τ_0 can be expressed in two ways as [11,12]:

$$\tau_0 = \epsilon_V \epsilon_{C0} \rho_0 / \langle x\rangle = \epsilon_V \epsilon_{C\infty} \rho_0 \langle x^{-1}\rangle, \tag{14}$$

where ϵ_{C0} and $\epsilon_{C\infty}$ are the zero- and infinite-frequency limits of the purely conductive-system dielectric quantity $\epsilon_C'(\omega)$ defined earlier. The second equation applies only when the low-τ end of the DRT is cut off, so $\langle x^{-1}\rangle$ is not infinite; otherwise, $\epsilon_{C\infty} = 0$. It is important to use ρ_0 rather than σ_0 in these equations in order to treat properly situations where $\sigma_0 \neq 1/\rho_0$ [13].

When $\rho_\infty \neq 0$, Eq. (14) must be replaced by [9–11]:

$$\tau_{0,S} = \epsilon_V (\epsilon_{C0})_S \rho_0 / \langle x\rangle_S, \tag{15}$$

where $\langle x\rangle_S \equiv \langle x\rangle(1 - W_\infty)$. Thus $\langle x\rangle_S \to 0$ at high temperatures where $W_\infty \to 1$ and simple Debye response is approached. Further, in this limit $\langle x\rangle \to 1$. The quantity W_∞ will always be defined here for the CMR, not CMRI, situation. Note that since $(\epsilon_{C\infty})_S = 0$ for the present situation with or without cutoff, we have no choice here but to use Eq. (15) to relate τ_0 to other relevant quantities. The above replacement of ϵ_∞ by the non-zero quantity ϵ_{C0} requires changes in several of the equations used by Funke in deriving the CMR [1,2].

The CSD1 expression of Eq. (11), a form of the corrected modulus-formalism response approach, is written in normalized form and so can be used directly for normalized data. Consider now the $\rho_\infty = 0$ case implicitly considered by Moynihan and associates [16,17] in deriving their modulus-formalism results. Then the unnormalized expression corresponding to Eq. (11) is, from Eq. (5), when written at the modulus level, $M_1(\omega) = i\omega\epsilon_V \rho_0 I_1(\omega)$, which may be expressed in a simpler form on using Eq. (14) to eliminate $\langle x\rangle_0$ as:

$$M_1(\omega) = [1 - I_0(\Omega)]/(\epsilon_{C0})_0, \tag{16}$$

In the original and later versions of the modulus formalism approach, in place of the quantity $(\epsilon_{C0})_0$ either $\epsilon_{D\infty}$ or ϵ_∞ was incorrectly used [16–20,45]. As shown by Eq. (14), we can replace $(\epsilon_{C0})_0$ in Eq. (16) by $(e_{C\infty})_0$ $\langle x\rangle\langle x^{-1}\rangle$. For all physically realizable situations, low-τ cutoff will be present [12,14], so $(\epsilon_{C\infty})_0$ will always be non zero when $\rho_\infty = 0$.

It is now clear that the normalization quantity to be used for frequency and time values is not the Eq. (13) $\langle\tau_\sigma\rangle$, as specified by Funke [1,2], but the τ_0 of Eq. (15) for the CMR. Further, Eq. (15) cannot be used to calculate a value of τ_0 even when $\langle x\rangle$ and ρ_0 values are known. Values of ρ_0 and σ_∞ and the normalized model are insufficient to allow $\sigma(\omega)$ to be calculated because τ_0 cannot be obtained from Eq. (15) without a value of ϵ_{C0} being known, and this quantity can only be obtained from unnormalized data. To estimate τ_0, one must give up the appealing but incorrect approach of using some value of ϵ_∞ in Eq. (13) and instead estimate τ_0 directly by, for example, comparison of normalized and unnormalized σ data (see the examples presented below). Because a value of τ_0 is required to convert Ω values to ω ones, until an estimate of τ_0 is available, the transformation of complex $\sigma(\Omega)$ data to the complex $\epsilon(\omega)$ level to obtain estimates of $\epsilon'(0)$ ($\equiv \epsilon_{C0} + \epsilon_{D\infty}$) and $\epsilon'(\infty)$ ($= \epsilon_{D\infty}$ for the CMR) cannot be carried out.

6.2. Fitting of CKN data and scaling

The Funke MIA simulation/fit results of CKN data mentioned above [1] are difficult to compare with the actual CKN data curves for $T = 478$, 453, and 423 K presented in Fig. 3b of Ref. [1], both because the simulation dealt with temperatures different from these and because the simulation plot involved a log(σ', Ω-cm) scale rather than the log($\sigma' T$, Ω-cm/K) scale employed for the data plots. Comparison of the simulation with the data nevertheless shows that they are qualitatively similar, although the thermal activation parameter values cited

by Funke for $\sigma_\infty(T)$ do not lead to the actual $\sigma_\infty(T)$ values shown for the CKN data curves.

Because Funke [1,2] used the MIA model and did not actually compare any simulation results directly with the CKN data, it seemed worthwhile to me to use the CMR for such comparison. Since the present instantiation of the CMR model in the LEVM fitting program allows direct fitting of data such as that for CKN, taking proper account of $\epsilon_{D\infty}$ as well, I asked Professor Funke to send me the full complex data for the three temperatures cited above. Because I received no reply to this request and did not receive these data sets, I decided to carry out a less ambitious program, but, hopefully, one which would still allow some quantitative evaluation of the adequacy of the CMR approach for describing these data sets.

First, the published CKN data graph was enlarged and three points on each of the lines for the above three temperatures were scaled from the enlargement, using a Gerber variable scale. The points were selected to define the low- and high-frequency saturation values and the value of $\log(\sigma' T,\ \Omega\text{-cm/K})$ at $\log(\nu, \text{Hz}^{-1}) = 11$, approximately the middle of the large-slope parts of the curves. In Fig. 10, the actual fit curves are shown for $T = 478$ and 423 K and are compared to points scaled off the data graph at frequencies near the beginning and end of the large-slope regions. It should be emphasized that the CMR model was forced to fit the high- and low-frequency saturation regions as well as a point between them quite accurately. For each temperature, these fit values then allowed estimates of σ_0, σ_∞, and τ_0 $(= \tau_{0S})$ values to be obtained. Although the results are all necessarily approximate, they are sufficiently accurate, I believe, to allow some reasonable conclusions to be reached about the applicability of the CMR model for these data.

First, it was found, in agreement with the previous work [1], that the three σ_∞ values could be fitted with $\sigma_\infty \simeq (A/T)\ \exp(-\Delta/k_B T)$ on using LEVM with proportional weighting. The S_F value found was about 0.011, and the estimates of the parameters were $\Delta \simeq k_B \cdot 2366$ K, in good agreement with the value quoted by Funke of $k_B \cdot 2380$ K, and $A \simeq 4.75 \times 10^4$ K/ohm-cm, about 49 times smaller than the corresponding Funke value, one which perhaps involved a misprint. As mentioned by Funke [1], $\sigma_0(T)$

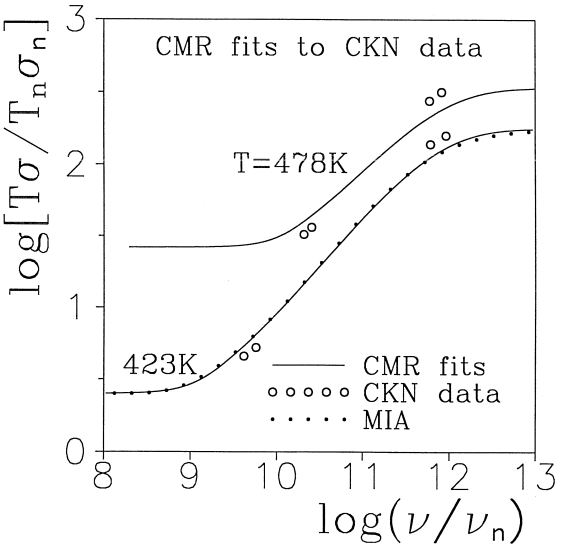

Fig. 10. Comparison of CMR fits to CKN real-part conductivity data for two different temperatures. Fitting parameters of the CMR curves were adjusted to yield agreement with the data at both the low and high ends of the response and at $\log(\nu/\nu_n) = 11$. Also some intermediate CKN data points are shown explicitly. In this graph, the normalization quantities are $T_n = 1$ K; $\sigma_n' = 1\ (\Omega\ \text{cm})^{-1}$; and $\nu_n = 1$ Hz. The 423-K MIA curve was calculated with the same parameter values as those for the corresponding CMR one except for the adjustment of its frequency normalization parameter, as discussed in the text. The open-circle points just below and above the two solid-line curves show associated CKN data values for these two temperatures.

does not follow Arrhenius behavior but was suggested to follow the empirical Vogel–Fulcher–Tammann equation [46–48]. Here, fitting led to an estimate of the VFT characteristic temperature parameter, T_0, of about 304 K.

It is difficult to obtain adequately accurate values of τ_0 by the present graphical approach, and this quantity is the least well determined of those estimated here. Nevertheless, an Arrhenius fit with T^{-1} present in the pre-exponential factor led to an S_F value of about 0.08 and an activation-energy factor of about $k_B \cdot 7825$ K. The pre-exponential factor was of the order of 10^{-16} but was very poorly determined. Finally, estimates of ϵ_{C0} of about 7.8, 9.2, and 10.4 for $T = 478$, 453, and 423 K, respectively, were obtained. These values are too irregular to allow one to decide unambiguously between temperature independence, Curie behavior, or some other smooth dependence, but they do indicate that

ϵ_{C0} is likely to vary far less with temperature than does τ_0. Incidentally, the $\epsilon_{C\infty}$ values obtained by transformation of CMR to CMRI response were about 1.8, 1.6, and 1.2 for the above temperatures, respectively. Although they show only relatively small dependence, in agreement with an earlier analysis [12], it is clearly opposite to that of ϵ_{C0}.

Arrhenius fitting of the τ_0 data without the T^{-1} factor led to a slightly better fit, to an estimate of the activation energy parameter of $k_B \cdot 8273$ K and to a statistically meaningless estimate of the pre-exponential factor of 2×10^{-19}. Consider the behavior of a material with $\rho_\infty = 0$ at sufficiently low temperatures that the shape of the associated DRT is temperature independent over an appreciable range. Then, $\langle x\rangle$ would also be temperature independent, and Eq. (14) puts some interesting constraints on τ_0 and ρ_0. First, if ϵ_{C0} is temperature independent, then τ_0 and ρ_0 must have the same temperature dependence in this region. Alternatively, if ϵ_{C0} should be proportional to T^{-1}, then τ_0 and ρ_0/T must have the same temperature dependence, leading to the absence of a T^{-1} factor for τ_0 if the ρ_0 pre-exponential factor is $\propto T$. In both cases, the absence of a T^{-1} factor for τ_0 is plausible.

Also shown in Fig. 10 is a 423 K line for the MIA, one in which its τ normalization value, say $\tau_{\rm om}$, has been set to $\tau_0\pi/2$ in order to force its predictions to agree as well as possible with those of the CMR model. This factor largely eliminates the offset between such curves as those shown in Fig. 1. It is worth recalling, however, that Funke [1] has defined a low-frequency approximation for the MIA model by eliminating the second E_1 term on the right of Eq. (4) and has pointed out that the slope of the resulting curve continually increases towards unity as the frequency increases but never reaches that value. By contrast, it turns out that for very small values of W_∞, such as that for the 10^{-5} curve of Fig. 1, the CMR slope soon reaches an approximately constant value which is maintained until the approach to the high-frequency plateau. Therefore, there is no constant factor, such as $\pi/2$, which allows the two curves to yield the same results over a sufficiently wide frequency range. The above slope behavior of the exact CMR model is likely to be more appropriate for matching real data than that of the low-frequency form of the MIA.

Examination of Fig. 10 shows significant differences between the data points and the curves. The data curves are slower to begin their rise from σ_0 and faster to reach high- frequency saturation. Thus, their mid-range slopes are larger than those of the CMR or of the shifted MIA. The faster approach of the data to high-frequency saturation has already been noted by Funke [1], who provides some microscopic physical justification for the difference. The MIA curve agrees closely here with the corresponding CMR one except where the high-frequency saturation begins. This discrepancy is associated with the difference in slopes illustrated in Fig. 2 between these two approaches.

Although the CMR and MIA models do not describe the CKN data of Fig. 10 very well, it should be pointed out that if τ_0 were determined by the onset of the non-zero slope region, rather than at its middle, different values of τ_0 would be found (a measure of the inadequacy of the model), but such a shift would allow the initial-rise portions of the curves towards a constant slope to fit the data appreciably better, at the expense, of course, of worse fits at the high end. This behavior points up an interesting anomaly: in [2] it is demonstrated that a (shifted) low-frequency-approximation MIA curve does not fit the low frequency region of a master curve which, it is claimed, applies for many different materials, including CKN. In contrast, the present results indicate that the CMR can apparently fit the lower-frequency part of the CKN data reasonably well without the broadening adjustments required to obtain a good fit in Ref. [2]. Nevertheless, one must conclude that neither here nor in the Funke work [1,2,5,6] has adequate evidence been presented that shows that the CMR response model (or the MIA one) can represent experimental data in much more than a qualitative fashion. To do so for the CMR, one would want to fit both the real and imaginary parts of appropriate frequency-response data simultaneously using a CNLS approach [8].

In [7], B. Roling has presented a detailed study of the scaling properties of a variety of materials. He found that scaling to make frequency response curves overlap for different glassy materials and temperatures, and so to generate a master curve, involved the factor $[\omega f/\sigma_0 T]$, where f was either a factor proportional to the number of mobile ions or was taken as an adjustable free parameter, possibly temperature independent. We see from Fig. 1 that

indeed normalized CMR curves show essentially the same normalized frequency response in the low-frequency regions well below the high-frequency plateau. Therefore, the Roling factor should be proportional to the τ_0 of Eq. (15), the proper scaling factor for data which either involve or do not involve $\rho_\infty \neq 0$. Note that even when $\rho_\infty = 0$, there will always be a high-frequency plateau because of cut-off effects, as already discussed. If f is taken temperature independent, Roling's result follows from Eq. (15), when τ_{0S} and ρ_0 have the same temperature dependence, only if $[\epsilon_{C0}T/[(1-W_\infty)\langle x\rangle]$ is temperature independent. Although it is plausible that ϵ_{C0} might show Curie temperature dependence under some conditions, the product $\langle x\rangle_S \equiv (1-W_\infty)\langle x\rangle$ is never temperature independent unless W_∞, is; certainly not the case in general or for CKN.

If we define $w \equiv \log(W_\infty)$, an approximate fitting relation between $\langle x\rangle_S$ and w for the CMR is $\langle x\rangle_S = A\tan^{-1}(Bw^C) + D + Ew$, where the fit parameters are given approximately by 2, 0.81, 0.82, −0.03, and 0.11, for A through E, respectively. For $0 < w \leq 10^6$ the S_F for the fit was about 0.0019, an adequately small value. Note that although $\langle x\rangle_S \to 0$ as $W_\infty \to 1$ for the CMR, when one eliminates the effect of ρ_∞ by transforming the data to $I(\Omega)$, $\langle x\rangle \to 1$ in this limit, the expected value for simple Debye response. In previous work on $z\mathrm{AgI}+(1-z)(0.525\mathrm{Ag_2S}+0.475\mathrm{B_2S_3{:}SiS_2})$ glasses [12,45], it was shown that the approach to saturation of σ_0 at high temperatures could be explained virtually entirely by the change in distribution shape toward Debye response as the temperature increased. It seems likely that similar changes may explain much of the deviation of the CKN σ_0's from Arrhenius behavior. Finally, note that the presence of the $(1-W_\infty)$ term in Eq. (15) ensures that as the temperature increases τ_{oS} will eventually become much larger than the dielectric relaxation time, which involves $\epsilon_{D\infty}$, so that the latter will then dominate the response.

7. Definitions of acronyms and of principal symbols

CKN	Abbreviation designating calcium–potassium–nitrate material, here of composition $0.4\mathrm{Ca(NO_3)_2}\cdot 0.6\mathrm{KNO_3}$
CMR	Concept of mismatch and relaxation. The CMR response model is here defined by Eqs. (1) and (3)
CMRI	CMR response with the effect of $\rho_{N\infty}$ eliminated. See Eqs. (5) and (6)
CSD	Conductive-system dispersion
CSDn	Two types of CSD response with $n=0$ or 1; see Eqs. (8)–(10)
DRT	Distribution of relaxation times, τ.
KWW	Kohlrausch–Williams–Watts response model
KWWn	Two types of KWW CSD response denoted by n, where $n = 0$ or 1
LEVM	The complex-nonlinear-least-squares fitting program used herein.
MIA	Mirror image approach; a fitting model, see Eq. (4). The approximate MIA model is one in which the second E_1 term is eliminated from Eq. (4)
NCL	Nearly constant loss
x	τ/τ_x
$\langle x^m\rangle_n$	Dimensionless moment of a distribution; see Eq. (9)
y	$\ln(x)$
E_1	Exponential integral of the first kind; see Eq. (1)
$g(\Theta)$	Microscopic relaxation factor; see Eq. (2)
$F_n(y)$	A normalized DRT involving the logarithmic variable y. Equal to $xG_n(x)$
$G_n(x)$	A normalized DRT associated with $I_n(\Omega)$. See Eq. (8)
$I_n(\Omega)$	Normalized conductive-system resistivity dispersion function; does not include any effects of a non-zero ρ_∞. See Eqs. (5) and (8).
$M(\omega)$	Complex modulus function, equal to $i\omega\epsilon_V\rho(\omega) = 1/\epsilon(\omega)$.
$M_N(\Omega)$	Normalized modulus function, equal to $i\Omega\rho_N(\Omega) = 1/\epsilon_N(\Omega)$
N	Number of discrete points used in defining a DRT (≤ 19 for LEVM)
S_F	Standard deviation of fit residuals. For proportional weighting, it is the relative standard deviation of the fit or, equivalently, the standard deviation of the relative residuals
$W(\Theta)$	Basic variable of the CMR; a time-dependent ion correlation factor.
W_∞	Abbreviation of $W(\infty)$

$W_N(\Theta)$	$W(\Theta)/W_\infty$
$\Delta\rho_N(\Omega)$	$\rho_{N0} - \rho_{N\infty}$
Θ	Normalized temporal variable: t/τ_x
Ω	Normalized frequency variable: $\omega\tau_x$
β	$\beta = \beta_0$, the fractional exponent in KWW0 temporal response; see Eq. (7)
$\epsilon(\omega)$	Full dielectric response function. In the absence of true dielectric-system dispersion in the frequency range of interest, $\epsilon(\omega) = \epsilon_C(\omega) + \epsilon_{D\infty}$
$\epsilon_C(\omega)$	CSD dielectric response arising solely from mobile charges
ϵ_{C0}	Abbreviation for $\epsilon_C(0)$
$\epsilon_{C\infty}$	Abbreviation for $\epsilon_C(\infty)$
$\epsilon_{D\infty}$	High-frequency-limiting true dielectric constant arising from dipolar effects
ϵ_∞	Abbreviation for $\epsilon(\infty) \equiv \epsilon_{C\infty} + \epsilon_{D\infty}$
$\epsilon_N(\Omega)$	Normalized full dielectric constant, equal to $\epsilon_V\epsilon(\omega)/(\sigma_0\tau_x)$
ϵ_V	Permittivity of vacuum
ν	Frequency in Hz; $\omega/2\pi$
$\rho(\omega)$	Translational resistivity, a complex quantity
ρ_0	Abbreviation for $\rho(0)$
$\rho_N(\Omega)$	$\rho(\Omega)/\rho(0)$
ρ_{N0}	Abbreviation of $\rho_N(0)$
$\rho_{N\infty}$	Abbreviation of $\rho_N(\infty)$
$\sigma(\omega)$	Translational conductivity, $\sigma(\omega) = \sigma'(\omega) + i\sigma''(\omega)$
$\sigma_N(\Omega)$	$\sigma(\Omega)/\sigma(0)$, equal to $\{p'(\Omega)\}^{-1}$
τ_{min}	The minimum relaxation time for a cut off DRT
τ_x	Characteristic relaxation time of a response model
τ_0	Designation of τ_x for the CMR response model
$\phi(t)$	Macroscopic relaxation function; see Eq. (7)

Acknowledgements

It is a pleasure to thank Professor K. Funke for stimulating E-mail correspondence and for his kindness in answering questions about his work.

This is a brief outline of the CMR computational method instantiated in LEVM. First, in order to use Eq. (3) it is necessary to invert Eq. (1) so that one has available the function $W_N(\Theta)$ instead of $\Theta(W_N)$. Such inversion needs to be carried out very accurately for some values of Θ, especially for $W_\infty \ll 1$. To do so, I used the van Wijngaarden–Dekker–Brent root-finding method, one which has the advantage that it continues calculating until a specified accuracy is achieved [49]. In addition, I used a program which allowed very accurate calculation of the E_1 function [50]. It is straightforward to calculate the derivative in Eq. (3) from Eq. (1), and this approach was one of those used. An alternative, employed by Funke and associates for real-part calculations [21], and by me for calculation of both parts of $\sigma_N(\Theta)$, is to first integrate Eq. (3) by parts. This approach leads initially to the necessity of evaluating a cosine, outside the integral, at infinity, an ugly requirement. But, as used by Funke [21], the function outside the integral can be replaced by an equivalent term inside it, resulting in the following alternative to Eq. (3):

$$\sigma_N(\Omega) = W(0) + i\Theta\int_0^\infty [W_N(\Theta) - 1]\exp(-i\Omega\Theta)\mathrm{d}\Theta. \tag{A.1}$$

For both Eqs. (3) and (A.1) there still remains the computational problem of accurately integrating a function involving rapidly oscillating sines and cosines when their arguments are large. Although Funke et al. used a specific canned program for their integration which took explicit account of such oscillation, I employed an open version of a Romberg integration routine [Ref. [49], pp. 134–137], one which continues to add integration points until specified accuracy is achieved. Finally, in order to limit computational time, it is only necessary to use such integration up to a maximum Θ value, Θ_{max}, which, in some ranges is usefully taken to be a function of both Θ and W_∞. Since the non-sinusoidal parts of the arguments under the integral sign for both Eqs. (3) and (A.1) can be shown to approach $\exp(-\Theta)$ very accurately for large Θ, integration from Θ_{max} to ∞ can be carried out analytically. As a check of both the Funke and the present methods, I found, for example, agreement between them for $\sigma'(\Omega)$ to a large number of significant figures for the choices $W_\infty = 10^{-8}$ and $\Theta = 10^7$.

References

[1] K. Funke, Z. Phys. Chem. 206 (1998) 101.
[2] K. Funke, B. Roling, M. Lange, Solid State Ionics 105 (1998) 195.
[3] K. Funke, Prog. Solid State Chem. 22 (1993) 111.
[4] K. Funke, private communication, 8 August, 1998.
[5] K. Funke, private communication of preprint, (See Ref. 6) received 28 January, 1999.
[6] K. Funke, D. Wilmer, Solid-state Ionics V, Fall Meeting, 30 November–4 December, 1998, Boston, MA,, Proceedings of the Materials Research Society, Warrendale, PA, Vol. 548, 1999.
[7] B. Roling, Solid State Ionics 105 (1998) 185.
[8] J.R. Macdonald, L.D. Potter Jr., Solid State Ionics 23 (1987) 61, The latest version of the LEVM fitting program, V. 7.1, may be obtained at no cost from Solartron Instruments, Victoria Road, Farnborough, Hampshire, GU147PW, England; E-mail, attention Mary Cutler, lab_info@solartron.com. More details about the program appear in http://www.physics.unc.edu/~macd/.
[9] J.R. Macdonald, J. Non-Cryst. Solids 197 (1996) 83.
[10] J.R. Macdonald, Erratum, J. Non-Cryst. Solids 204 (1996) 309, GD in Eq. (A2) should be G_{CD}, essentially the present G_1 quantity.
[11] J.R. Macdonald, J. Non-Cryst. Solids 212 (1997) 95, The symbol σ_0 should be removed from the right end of Eq. (12); Eq. (7) in this work does not apply to Eqs. (3) and (4) when $\rho_{C\infty} \neq 0$ (see Ref. 9, above); and the word 'frequency' in the third line from the bottom of the second column of p. 111 should be 'temperature'.
[12] J.R. Macdonald, J. Appl. Phys. 84 (1998) 812, The word 'out' in the third line from the bottom of the first column on p. 820 should be 'but'.
[13] J.R. Macdonald, Braz. J. Phys. 29 (1999) 332. This paper may be downloaded from http://www.sbf.if.usp.br/WWW_pages/Journals/BJP/Vol29/Num2/index.htm
[14] J.R. Macdonald, Solid State Ionics 25 (1987) 271.
[15] J. R. Macdonald, Phys. Rev. B 49 (1994-II) 9428.
[16] P.B. Macedo, C.T. Moynihan, R. Bose, Phys. Chem. Glasses 13 (1972) 171.
[17] C.T. Moynihan, L.P. Boesch, N.L. Laberge, Phys. Chem. Glasses 14 (1973) 122.
[18] C.T. Moynihan, J. Non-Cryst. Solids 172–174 (1994) 1395.
[19] C.T. Moynihan, J. Non-Cryst. Solids 203 (1996) 359.
[20] C.T. Moynihan, Solid State Ionics 105 (1998) 175.
[21] K. Funke, private communication, 15 October, 1998.
[22] P. Maass, M. Meyer, A. Bunde, Phys. Rev. B 51 (1995) 8164.
[23] D. Knodler, P. Pendzig, W. Dieterich, Solid State Ionics 86–88 (1996) 29.
[24] R. Kohlrausch, Pogg. Ann. der Phys. und Chemie 91 (2) (1854) 179.
[25] G. Williams, D.C. Watts, Trans. Faraday Soc. 66 (1970) 80.
[26] G. Williams, D.C. Watts, S.B. Dev, A.M. North, Trans. Faraday Soc. 67 (1971) 1323.
[27] J.R. Macdonald, J. Appl. Phys. 62 (1987) R51.
[28] J.R. Macdonald, J. Appl. Phys. 82 (1997) 3962.
[29] K. Funke, R. Hoppe, Solid State Ionics 40–41 (1990) 200.
[30] Discussion session on glassy ionics, J. Non-cryst. Solids 131–133 (1991) 1113–1122.
[31] J.P. Dyre, J. Non-Cryst. Solids 135 (1991) 219.
[32] S.R. Elliott, J. Non-Cryst. Solids 170 (1994) 97.
[33] B. Roling, A. Happe, K. Funke, M.D. Ingram, Phys. Rev. Lett. 78 (1997) 2160.
[34] J. Schrama, Ph.D. Thesis, University of Leiden, Netherlands, 1957.
[35] K. Funke, J. Hermeling, J. Kumpers, Z. Naturforsch 43a (1988) 1094.
[36] W. Dieterich, D. Knodler, P. Pendzig, J. Non-Cryst. Solids 172–174 (1994) 1237.
[37] A. Pimenov, P. Lunkenheimer, H. Rall, B. Kohlhaas, A. Loidl, Phys. Rev. E 54 (1996) 6760.
[38] J.R. Macdonald, J. Chem. Phys. 102 (1995) 6241.
[39] J.R. Macdonald, Computers in Physics 9 (1995) 546.
[40] J.R. Macdonald, Electrically Based Microstructural Characterization, Proceedings Materials Research Society Fall Meeting, Boston, MA, November 1995, Vol. 411, Materials Research Society, Warrendale, PA, 1996.
[41] B. Munro, M. Schrader, P. Heitjans, Ber. Bunsenges Phys. Chem. 96 (1992) 1718.
[42] P. Jeevanandam, S. Vasudevan, J. Chem. Phys. 109 (1998) 8109.
[43] W.K. Lee, J.F. Liu, A.S. Nowick, Phys. Rev. Lett. 67 (1991) 1559.
[44] J.R. Macdonald, J. Non-Cryst. Solids 210 (1997) 70.
[45] K.L. Ngai, A.K. Rizos, Phys. Rev. Lett. 76 (1996) 1296.
[46] H. Vogel, Phys. Z. 22 (1921) 645.
[47] G.S. Fulcher, J. Am. Ceram. Soc. 8 (1925) 339.
[48] V.G. Tammann, H. Hesse, Z. Anorg. Chem. 156 (1926) 245.
[49] W.H. Press, S.A. Teukolsky, W.T. Vetterling, B.P. Flannery, Numerical Recipes in FORTRAN, Cambridge University Press, 1992, pp. 352–354.
[50] W.J. Thompson, Atlas For Computing Mathematical Functions, Wiley, New York, 1997, pp. 60–62.